博 士 論 文

Pharmacological study of teriparatide on ovariectomy-induced hyperalgesia in rats
(卵巣摘除ラットモデルを用いた骨粗鬆性痛覚過敏に対するテリパラチドの薬理作用の解明)

令和 2 年 3 月申請

北海道大学

大学院歯学研究科口腔医学専攻

田　中　智　哉

目次

Introduction

More than 80% of osteoporotic patients reportedly have low back pain, which leads to disability and progression of bone and muscle weakening, and eventually reduces quality of life[1,2]. This osteoporotic pain occurs in patients regardless of obvious bone fractures in the vertebrae and other sites. A possible causative mechanism of osteoporotic pain is chronic neuronal excitement in intraosseous sensory nerve systems by acids and inflammatory cytokines produced by the activation of osteoclasts, as well as monocytes and macrophages, due to estrogen deficiency[3,4]. This mechanism has been proposed to be involved in cancer-associated bone pain patients with bone metastases[5]. Osteoporotic patients may also experience pain originating from collapsed vertebral bodies, degenerated intervertebral disc and facet joints[6]. Chronification of osteoporotic pain involves hypoactivity of the descending inhibitory nerve system that modulates ascending pain-transmission in the spinal cord with the decreased expression of serotonin receptors[3,7].

Anti-osteoporotic agents have been reported to be clinically and experimentally effective against bone pain. Bisphosphonates (BPs) exerted pain-modulating effects by suppressing osteoclasts, monocytes, and macrophage activity to curb the production of acids and inflammatory cytokines[3,8]. It has also been reported that the BP drug minodronate exerts a pain-modulating effect by inhibiting the purinergic P2X2/3 receptor[9]. Calcitonin depresses bone resorption and osteoclast activity by acting on osteoclast surface receptors. It has also been reported that calcitonin exerts its pain-modulating effect by depressing osteoclasts and correcting the decline in serotonin receptor activity that causes hypoactivity of the descending inhibitory system[7,10,11]. To study the antinociceptive effect of anti-osteoporotic agents, ovariectomized (OVX) animals, a widely-used osteoporosis animal model, are often used. It is well established that OVX animals show not only loss of bone density but also hyperalgesia to heat and mechanical stimuli[8,10-13]. It has been reported that estradiol improves the pain-related behavior induced OVX, indicating that estrogen deficiency influences the response to heat and mechanical stimuli[11-13]. Also, It has been reported that the pain-related behavior induced OVX is improved not only by BP and calcitonin but also by pregabalin and morphine[8,10,11,14].

Teriparatide (TPTD; the 1-34 fragment of human parathyroid hormone [PTH]) exerts a bone anabolic effect and is a clinically effective therapeutic agent for osteoporosis by acting on PTH 1 receptor (PTH1R) in osteoblast-lineage cells, promoting the proliferation, differentiation, and survival of bone-forming osteoblasts. Accumulated epidemiological studies

have reported that TPTD treatment suppresses the onset and modulates the exacerbation of back pain in osteoporotic patients[15-20]. TPTD therapy was also effective against post-vertebral fracture pain[21-23] and incurable back pain in patients treated with BPs[24]. Improvement of back pain by TPTD appeared to be observed in earlier stages of the treatment than with calcitonin treatment[25]. However, despite the existence of multiple clinical reports as mentioned above, the pharmacological mechanism of the anti-osteoporotic pain effect of TPTD remains unclear.

This study investigated the antinociceptive effect of TPTD in OVX rats. We conducted pain-related behavioral tests and transcriptome analyses in the dorsal root ganglia (DRG) collected from the model rats followed by bioinformatic analyses.

Materials and methods

Experimental animals

Ten-week-old female Sprague-Dawley rats were used for this study (Charles River, Kanagawa, Japan). The rats were maintained under light and dark cycles (12-12 h) and allowed to unrestricted access to tap water and food (CRF-1; Oriental Yeast, Tokyo, Japan). Cages were enriched with nesting material (Enviro-dri; Shepherd Specialty Papers, Watertown, TN, USA). The rats were allowed to acclimate to their environment for 10 days before the start of the experiments. The experimental study was approved by the Experimental Animal Ethics Committee at LSI Medience Corporation and Asahi Kasei Pharma Corporation and performed according to established guidelines for the management and handling of experimental animals.

Experimental design

Twelve-week-old rats were randomized by withdrawal latency in the plantar test and body weight into 2 groups: the OVX group (n=20) and the Sham group (n=10). Bilateral OVX or sham surgery was performed under anesthesia. In the sham surgery, the ovaries were exteriorized but not removed. Four weeks after surgery, the OVX group rats were further randomized into 2 groups: the OVX-vehicle group (n=8) and the OVX-TPTD group (n=8). Eight specimens in each group were selected by the average body weight and the results of the preceding plantar test (described in a following section) and subjected to further analyses. Accordingly, 8 rats close to the average latency in the plantar test were selected from the Sham group (n=10) and defined as the Sham-vehicle group. The rats received the following treatments for 4 weeks: subcutaneous administration of TPTD (Asahi Kasei Pharma, Tokyo,

Japan) at a dose of 30 μg/kg body weight 3 times a week (OVX-TPTD group) or subcutaneous administration of saline 3 times a week (Sham-vehicle and OVX-vehicle groups). All rats were sacrificed by exsanguination from the abdominal aorta under isoflurane anesthesia at the end of the experimental period. The fourth and fifth lumbar DRG (L4-5 DRG), right femur, and blood samples were then collected for further analyses (Figure 1). Two pain-related behavioral tests were performed as described below.

Figure 1

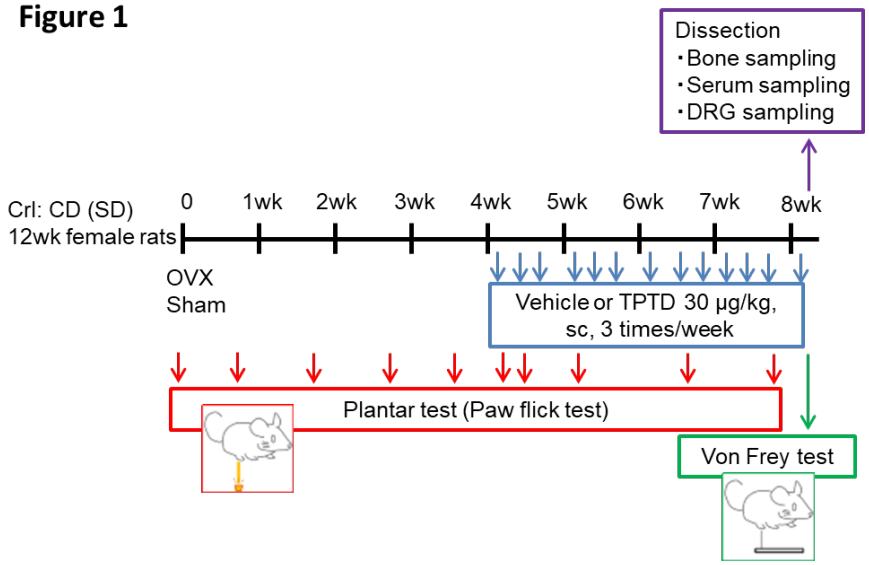

Figure 1. The time schedule of the experiments and sampling. The time schedule of OVX, TPTD administration, behavioral tests (plantar test and von Frey test), and sampling are shown.

Pain-related behavioral test

Plantar test

Rats were allowed at least two 30-min sessions to habituate to the test environment prior to behavioral testing. Thermal hypersensitivity was tested according to the Hargreaves procedure[26] using an analgesia meter (Plantar test 7370; Ugo Basile, Varese, Italy).

In brief, rats were placed in clear plastic boxes and allowed to acclimate. A constant-intensity radiant heat source was directed to the midplantar area of the left hind paw. The time from activation of the heat source until paw withdrawal was recorded as the paw withdrawal latency. The cut-off time was set for 15 seconds to avoid tissue damage. The plantar tests were conducted before surgery and 1, 2, 3, and 4 weeks after surgery to monitor hyperalgesia induced by OVX. After initial TPTD administration, the hypersensitivity was tested on the day of the first and second administration and every week to evaluate the effect on hyperalgesia. The plantar tests were conducted 5-6 h after the TPTD administration.

von Frey test

Rats were allowed at least two 30-min sessions to habituate to the test environment prior to behavioral testing. Mechanical sensitivity was measured using von Frey monofilaments on the left hind paw at the day of the final TPTD administration (5-6 h after administration). The von Frey withdrawal threshold was determined by adjusting the stimulus intensity between 1.0 and 26.0 g equivalents of force according to the up-and-down method[27].

In brief, rats were placed on mesh platforms in a plastic chamber. After acclimation for more than 5 min, filaments of sequentially increasing stiffness with initial bending force of 4.0 g were applied to the hind paw. A positive response was defined as the withdrawal of the hind paw to the stimulus. The withdrawal threshold was determined by sequentially increasing and decreasing the stimulus intensity.

Skeletal analyses

Measurement of the bone mineral density (BMD)

The right femur samples were collected and stored at −80 °C until analyses. Before measurement, the femur samples were immersed in saline at room temperature and removed the attached soft tissue. The BMD of the femur was measured using dual energy X-ray absorptiometry (DXA) equipment (DCS-600EX-3R; Aloka, Tokyo, Japan). The femur samples were placed on the scan table and scanned at a pitch of 1 mm and speed of 25 mm/min. The BMD (mg/cm^2) was calculated from the bone mineral content (mg) and bone area (cm^2)[28]. For the analysis, the femur was divided into three regions (proximal, shaft, and distal), and the BMD in each region was obtained.

Measurement of bone metabolic markers in serum samples

All rats were fasted for at least 6 h before sacrificing and blood sampling. Serum samples were obtained by centrifugation of the blood samples. The serum samples were aliquoted and stored at −80 °C until analyses. The level of osteocalcin, a bone formation marker, was determined using a rat osteocalcin ELISA kit (GE Healthcare Bioscience, Piscataway, NJ, USA). The level of C-terminal telopeptide of type I collagen (CTX), a bone resorption marker, was measured using a RatLaps ELISA kit (Nordic Bioscience Diagnostics, Copenhagen, Denmark). Both assays were performed according to the manufacturers' instructions.

Gene expression analyses

RNA isolation

Rats were sacrificed under isoflurane anesthesia, and the L4-5 DRG was readily dissected. The tissue samples were then immersed in 0.2 mL RNAlater (Thermo Fisher Scientific, Waltham, MA, USA) and stored at -80 °C until use. Total RNA from each sample was isolated using a RNeasy lipid-tissue mini kit with DNase I (QIAGEN, Hilden, Germany) to reduce contamination of genomic DNA prior to further analyses.

RNA sequencing (RNA-seq)

Sequence libraries were prepared using the TruSeq Stranded mRNA Sample Prep Kit (Illumina, San Diego, CA, USA). Sequencing was performed in the paired-end (100 x 2) mode on the HiSeq 2500 (Illumina) using a TruSeq SBS Kit v4-HS (Illumina). Sequenced reads data were mapped onto the *Rattus norvegicus* genome (rn6) using the TopHat software program v2.0.14 based on the Bowtie v2.2.5 and SAMtools v1.2 software programs. Fragments per kilobase per million (FPKM) values were computed by the Genedata Expressionist software program v9.1.4a (Genedata, Basel, Switzerland) (performed by Takara Bio, Shiga, Japan).

Metascape (http://metascape.org/) was used for the gene set enrichment analysis and functional annotation. A Metascape analysis is carried out with four sources: Gene Ontology (GO) Biological Processes, Reactome Gene Sets, Kyoto Encyclopedia of Genes and Genomes (KEGG) Pathway, and Comprehensive Resource of Mammalian protein complexes (CORUM). All analyses were performed with converting the input rat genes into their human orthologs as suggested by the Metascape manual.

We referred to the literature concerning bone pain[3-5], the Pain Genes Database[29] (http://www.jbldesign.com/jmogil/enter.html), and the gene list of Inflammatory Cytokines and Receptors RT^2 Profiler PCR Array (https://www.qiagen.com/us/shop/pcr/primer-sets/rt2-profiler-pcr-arrays/?catno=PARN-150Z#geneglobe) as the list of the genes associated with pain and inflammation. The gene expression profiles were presented as a heatmap using the gplots package in R v3.4.1. Hierarchical clustering of the gene expression was performed with Euclidean distance and the group average method.

The gene functional annotation profiles were presented as a heatmap based on the Metascape annotation data also using the gplots package in R. Similarly, hierarchical

clustering of the gene functional annotation was performed with Euclidean distance and the group average method. Two-dimensional functional mapping was performed with t-distributed stochastic neighbor embedding (t-SNE) using the Rtsne package (perplexity = 5) in R.

Quantitative real-time polymerase chain reaction (qPCR)

Isolated total RNA was subjected to cDNA synthesis with random primers using the SuperScript VILO cDNA Synthesis Kit (Thermo Fisher Scientific). The synthesized cDNA was used as templates for qPCR using the TaqMan Gene Expression Master Mix Kit and Taqman Gene Expression Assay (Thermo Fisher Scientific) on a QuantStudio 7 Flex System (Applied Biosystems, Waltham, MA, USA). Data were normalized against the corresponding expression levels of *Gapdh*. The TaqMan® Gene Expression assays used in this study are listed in Supplementary Table 1.

Supplementary Table 1. The TaqMan® Gene Expression assays used in this study.

Gene Symbol	Gene name	Assay ID
Adra2c	adrenoceptor alpha 2C	Rn00593341_s1
Bdnf	brain-derived neurotrophic factor	Rn02531967_s1
Calca	calcitonin-related polypeptide alpha	Rn01511353_g1
Calcrl	calcitonin receptor-like	Rn00562334_m1
Ccl21	chemokine (C-C motif) ligand 21	Rn01764651_g1
Gal	galanin/GMAP prepropeptide	Rn00583681_m1
Gapdh	glyceraldehyde-3-phosphate dehydrogenase	Rn01775763_g1
Grm8	glutamate receptor, metabotropic 8	Rn00573505_m1
Il11	interleukin 11	Rn00591721_m1
Il2rg	interleukin 2 receptor, gamma	Rn01752908_g1
Kcnj5	potassium channel, inwardly rectifying subfamily J, member 5	Rn01789221_mH
Ntf3	neurotrophin 3	Rn00579280_m1
P2rx1	purinergic receptor P2X, ligand-gated ion channel, 1	Rn00564454_m1
P2ry14	purinergic receptor P2Y, G-protein coupled, 14	Rn02532502_s1
Penk	proenkephalin	Rn00567566_m1
Ptger2	prostaglandin E receptor 2 (subtype EP2)	Rn00579419_m1
Pth1r	parathyroid hormone 1 receptor	Rn00571595_m1
Stoml3	stomatin (Epb7.2)-like 3	Rn01494610_g1
Tac1	tachykinin, precursor 1	Rn01500392_m1

Immunohistochemistry and microscopic systems

Rats were anesthetized and sacrificed via exsanguination from the abdominal aorta. The Lumbar vertebrae (L5) including the DRG were dissected and fixed in 4% paraformaldehyde at 4 °C for 2 days. Decalcification was carried out in 10% EDTA-2Na solution (Muto Pure Chemicals, Tokyo, Japan) for 2 weeks at 4 °C. After paraffin embedding, L5 DRG paraffin tissue blocks were cut into 5-μm-thick slices. Paraffin-embedded sections were de-paraffinized, and epitope retrieval was performed using a rice steamer at 95 °C for 30 min in 10 mM citrate buffer. The tissue sections were incubated in 5% bovine serum albumin (BSA) (Sigma-Aldrich,

St. Louis, MO, USA) in Tris-buffered saline with Tween 20 (TBS-T) (Takara Bio) for 30 min at room temperature and then washed. The samples were then incubated at 4 °C for 15 h in anti-PTH1R (1:200; Merck Millipore, Burlington, MA, USA) and anti-calcitonin gene-related protein (CGRP) (1:200; Enzo Life Sciences, Farmingdale, NY, USA). After being washed, the slides were incubated with anti-mouse IgG Alexa Fluor 488 (1:200; Thermo Fisher Scientific), anti-rabbit IgG Alexa Fluor 568 (1:200, Thermo Fisher Scientific), and DAPI (1:1000; Dojindo Laboratories, Kumamoto, Japan) for 1 h, followed by final washing. Finally, the slides were mounted with coverslips using Fluorescent Mounting Medium (Dako Denmark, Glostrup, Denmark).

Fluorescence images of the tissue sections were obtained by a vertical microscopy system with differential interference contrast, an ECLIPSE Ni (Nikon, Tokyo, Japan) equipped with objectives (Nikon), as follows: Plan Apo λ ×10 (numerical aperture [NA] = 0.45), Plan Apo λ × 20 (NA = 0.75), and Plan Apo λ ×40 (NA = 0.95). The fluorescence signals were obtained using the following filter sets: GFP-B (excitation: 460–500 nm, dichroic mirror (DM): 505 nm, emission: 510–560 nm; Nikon), TxRed (excitation: 540–580 nm, DM: 595 nm, emission: 600–660 nm; Nikon), and DAPI (excitation:340–380 nm, DM: 400 nm, emission: 435–485 nm; Nikon). Tiling fluorescence imaging to acquire the entire, high-contrast view of the tissue sections was carried out using a Plan Apo λ × 10 objective (NA = 0.45). The frame size of a single scan was 1280 × 1024 pixels with 8-bit color depth. The fluorescence and differential interference contrast images were sequentially acquired, with a pixel size of 0.64 μm. Image processing, including deconvolution, was performed using the imaging software program NIS-elements AR (Nikon).

In vitro analyses

Primary culture of rat DRG sensory neurons

DRGs were isolated from neonatal rats and digested in 1.25 mg/mL collagenase from *Clostridium histolyticum* (Sigma-Aldrich) and 0.2 mg/mL Deoxyribonuclease I from bovine pancreas (Sigma-Aldrich) in Ham's F-12 Nutrient Mix, GlutaMAX (F-12) (Thermo Fisher Scientific) for 45 min at 37 °C. Dissociated cells were spun through a 10% BSA cushion to remove debris. DRG neurons were plated onto poly-D-lysine-coated 96-well plates at a density of 50,000 cells per well and grown in F-12 supplemented with 1% fetal bovine serum (FBS) (Thermo Fisher Scientific) and 1% Penicillin-Streptomycin (PCSM) (Thermo Fisher Scientific).

After overnight culture, the medium was replaced with Neuro basal medium (Thermo Fisher Scientific) supplemented with B-27 (Thermo Fisher Scientific), GlutaMax (Thermo Fisher Scientific), 100 ng/mL nerve growth factor (NGF)-β from rat (Sigma-Aldrich), and 1% PCSM. The experiments were performed after three days of culture.

Measurements of cyclic AMP (cAMP) production and [Ca^{2+}] in DRG sensory neurons

Cultured DRG neurons were rinsed twice in Hank's Balanced Salt Solution (HBSS) containing 20 mM HEPES and 100 μM 3-Isobutyl-1-methylxanthine (IBMX) and then stimulated with TPTD or vehicle for 15 min at 37 °C. cAMP levels were determined with the Cyclic AMP EIA kit (Cayman Chemical, Ann Arbor, MI, USA) and VersaMax microplate reader (Molecular Devices, San Jose, CA).

Cultured DRG neurons were stained with a FLIPR Calcium-5 Assay Kit (Molecular Devices). TPTD or vehicle was then added to the wells, which were imaged with a FLIPR Tetra System (Molecular Devices) for 400 seconds.

Statistical analyses

All data are presented as the mean ± standard error of the mean.

The time-course data of plantar test in all groups is analyzed using a two-way ANOVA comparing with the differences among groups and time points. The OVX-vehicle group was compared with the Sham-vehicle group, and group differences were analyzed using Student's t test at each time point. The OVX-TPTD group was compared with the OVX-vehicle group, and group differences were analyzed using Student's t test at each time point after the confirmation of a significant difference by two-way ANOVA.

In von Frey test, skeletal analysis, and gene expression analyses, the OVX-vehicle group was compared with the Sham-vehicle group, and group differences were analyzed using Student's t test. The OVX-TPTD group was compared with the OVX-vehicle group, and group differences were analyzed using Student's t test.

In *in vitro* analyses, the effects of TPTD were investigated using Dunnett's test.

All p values of <0.05 were considered statistically significant.

Results

Effects of TPTD on the pain-related behavior in OVX rats

We first conducted two pain-related behavior tests (the Plantar test and von Frey test) in the three experimental groups of Sham-vehicle, OVX-vehicle, and OVX-TPTD (Figure 1 and 2). The paw withdrawal latency in the OVX-vehicle group gradually shortened and was significantly shorter than that in the Sham-vehicle group at 2 weeks after surgery on the plantar test ($p < 0.01$, *t*-test) (Figure 2a). Significant differences in the latency between these two groups were continuously observed up to eight weeks after the surgery, indicating that OVX induced prolonged hyperalgesia. At 4 weeks postoperatively, the OVX-TPTD group underwent TPTD administration (30 μg/kg) at 3 times a week for 4 weeks. At 6 h after the initial TPTD administration, the latency of the OVX-TPTD group immediately recovered to 40% of that in the Sham-vehicle group, a significant difference compared with that in the OVX-vehicle group ($p < 0.05$, t-test), until the end of the analysis (8 weeks after the surgery). The latency of the OVX-TPTD group showed an increasing trend at 4 weeks after the initial administration ($P=0.051$, *t*-test), and the antinociceptive effect remained about the same through the final day of administration.

Consistently, the von Frey test at 4 weeks after the initial administration (8 weeks postoperatively) showed that the OVX-vehicle group had a significantly lower withdrawal threshold to mechanical stimuli than the Sham-vehicle group ($p < 0.01$, *t*-test). The withdrawal threshold of the OVX-TPTD group was significantly higher than that of the OVX-vehicle group ($p < 0.01$, *t*-test), which indicated that TPTD recovered the threshold induced by OVX to approximately 30% of that in the Sham-vehicle group (Figure 2b).

Figure 2

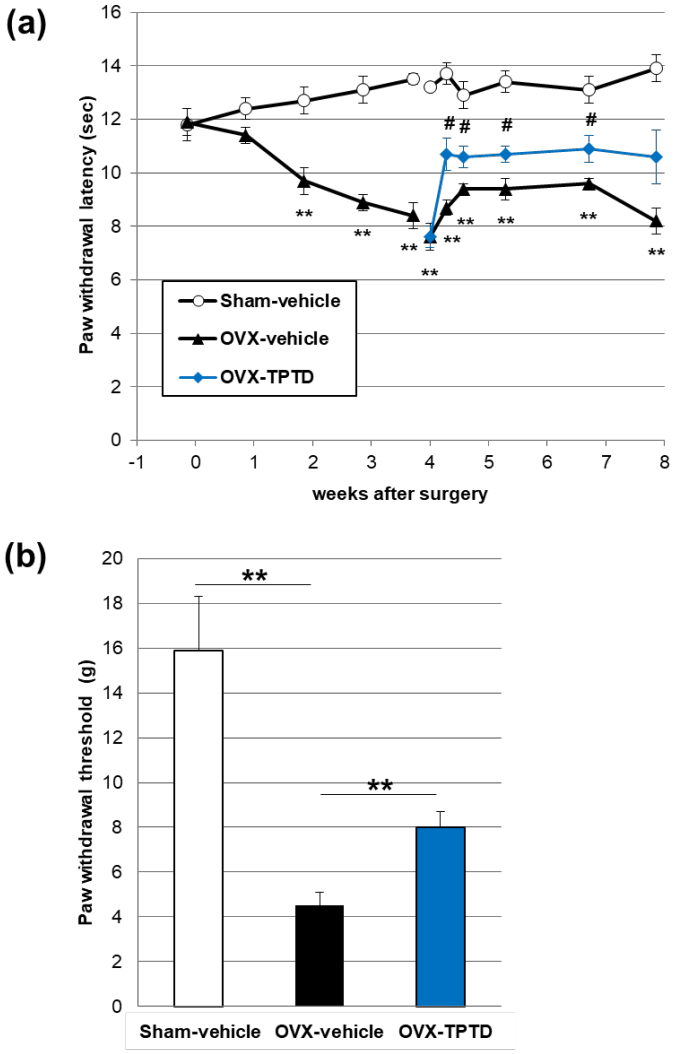

Figure 2. Antinociceptive effect of TPTD in OVX rats. (a) The plantar test was conducted during the period of the TPTD administration. TPTD administration (in the OVX-TPTD group) promptly and significantly recovered the reduced latency (shown in blue line). Significant difference: **p < 0.01 vs. sham, #p < 0.05 vs. OVX-vehicle group (a two-way ANOVA with a post-hoc Student's t test). (b) The von Frey test was carried out four weeks after the TPTD administration. The withdrawal threshold in the OVX-TPTD group (filled column in blue) was significantly higher than that in the OVX-vehicle group (filled column) at four weeks after the initial TPTD administration. Significant difference: **p < 0.01. Data are presented as the means ± S.E.M.

Bone anabolic effects of TPTD treatment in the OVX rats

We next confirmed the pharmacological effects of TPTD treatment on bones in the OVX rats (Figure 3) at four weeks after the initial TPTD treatment. The distal femoral BMD in the OVX-TPTD group was significantly greater than that in the OVX-vehicle group and comparable to those in the Sham-vehicle group (Figure 3a). The BMD of the femoral shaft in the OVX-TPTD group was higher than that in the OVX-vehicle group and Sham-vehicle group (Figure 3b). Therefore, the bone anabolic effects of TPTD treatment in this experimental regimen was confirmed.

The serum levels of osteocalcin and CTX were significantly augmented in the OVX-vehicle group compared with the Sham-vehicle group, suggesting that bone turnover was stimulated by OVX (Figure 3c, d). TPTD treatment up- and downregulated these bone formation and resorption makers, respectively, compared to those in the OVX-vehicle group, albeit not significantly.

Figure 3

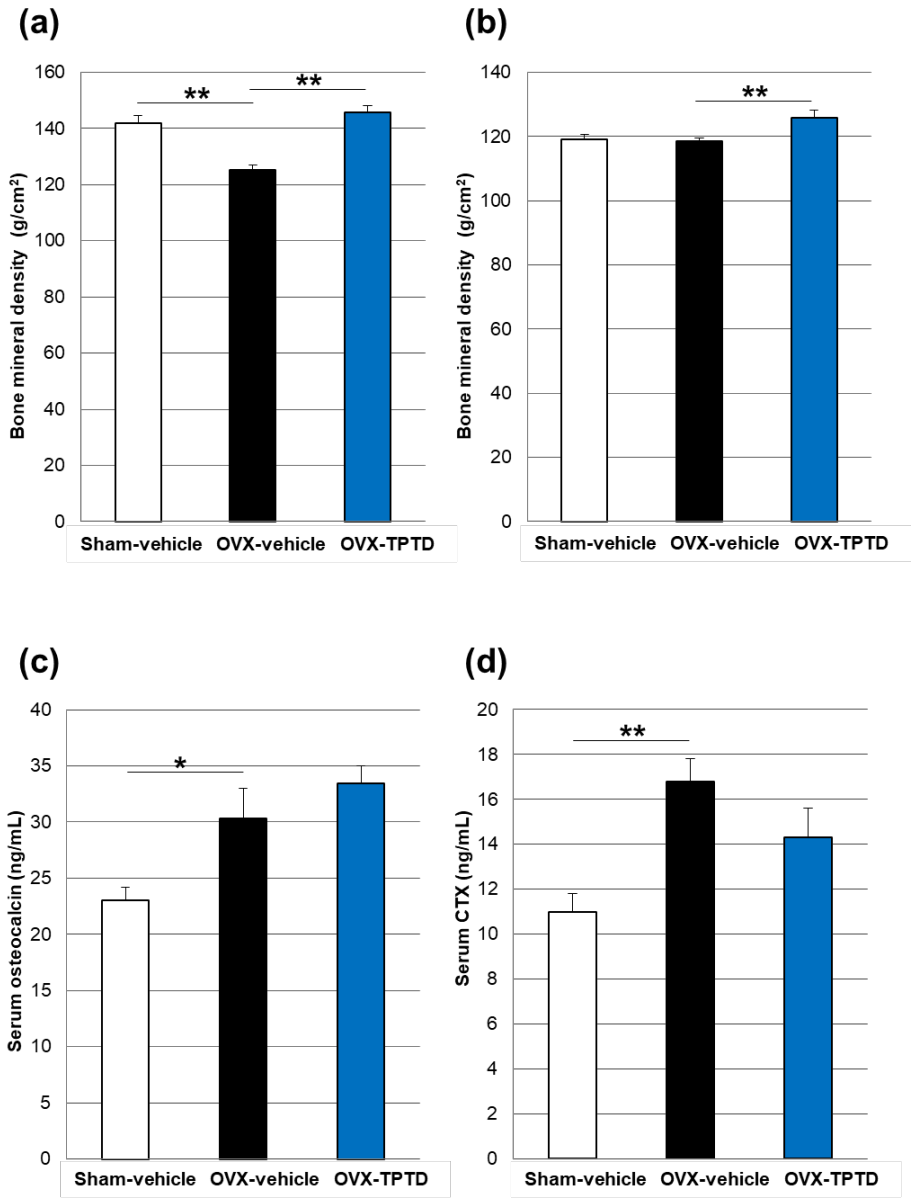

Figure 3. Anabolic effects of TPTD on bone metabolism in OVX rats. The BMD of the distal femur (a) and the femoral shaft (b) were measured at four weeks after the initial TPTD or vehicle administration. TPTD treatment significantly recovered the BMD in the OVX-TPTD group (filled column in blue). The serum osteocalcin concentration (c) and serum CTX concentration (d) were measured four weeks after the initial administration. Significant difference: *$p < 0.05$, **$p < 0.01$. Data are presented as the means ± S.E.M.

Existence of PTH1R in rat DRG neurons

To investigate whether or not DRG contains responsive cells to TPTD, we analyzed PTH1R by immunohistochemistry (Figure 4). We also used anti-CGRP as a marker of peptidergic neurons to dissociate neuronal subtypes in rat DRGs. PTH1R was detected in most neurons of the DRG, regardless of neuronal type. The transcription of *Pth1r* was detected by PCR in isolated rat DRG (Supplementary Figure 1).

Figure 4

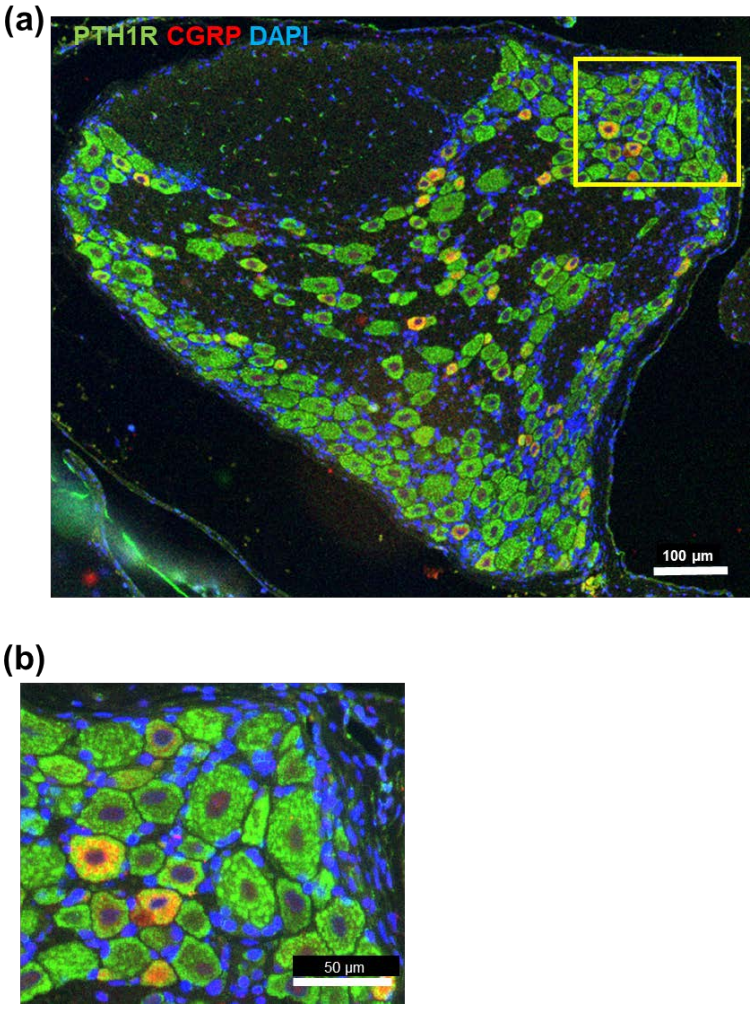

Figure 4. Detection of PTH1R in DRG neurons. (a) PTH1R was detected by fluorescence immunohistochemistry in DRGs, including CGRP-positive (a marker of unmyelinated C fiber neurons) and CGRP-negative neurons. (b) Higher magnification of the rectangle-bordered area shown in (a).

Supplementary Figure 1

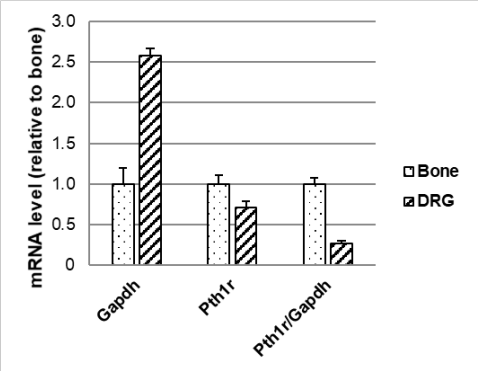

Supplementary Figure 1. The validation of the expression of *Pth1r* in DRG by PCR. Each mRNA level was shown when the same amounts of total RNA were used. Values are relative to bone samples and presented as the means ± S.E.M.

Changes in the DRG transcriptome profiles by OVX and TPTD treatment

To investigate the molecular basis of hyperalgesia associated with OVX and the antinociceptive effect of TPTD, we conducted a transcriptome analysis of RNA-seq in the DRG collected from rats in these experimental groups (Figure 5). Genes were identified by mapping onto the rat genome, and any gene that had 0 mapped reads for each sample was removed, resulting in 12,742 genes.

The expression of 619 genes differed significantly between the Sham-vehicle group and the OVX-vehicle group, while that of 464 genes differed significantly between the OVX-vehicle group and the OVX-TPTD group ($p < 0.05$, *t*-test). Among the significantly different genes, 182 and 179 had an absolute log2 (fold change) > 0.25 between the Sham-vehicle group and the OVX-vehicle group and between the OVX-vehicle group and the OVX-TPTD group, respectively.

Differentially expressed genes (DEGs) were functionally annotated and clustered by the GO Biological Processes, Reactome Gene Sets, KEGG Pathway, and CORUM using the Metascape webtool. The top 20 enriched terms or pathways are shown in Supplementary Figure 2a and b by their log10(p-values). The Metascape analysis revealed that the DEGs between the Sham-vehicle group and the OVX-vehicle group (182 genes) were significantly associated with tissue remodeling (GO:0048771) and neuroactive ligand-receptor interaction (KEGG:hsa04080) (-log10(p-values) > 6) (Supplementary Figure 2a), while the DEGs between

the OVX-vehicle group and the OVX-TPTD group (179 genes) were significantly associated with cytokine-mediated signaling pathways (GO:0019221) and the regulation of the response to cytokine stimuli (GO:0060759) (-log10(p-values) > 6) (Supplementary Figure 2b).

We next conducted an analysis focused on pain. The genes associated with pain and inflammation were selected from the DEGs mentioned in previous studies on bone pain[3-5], the Pain Genes Database[29], and the gene list of Inflammatory Cytokines and Receptors RT^2 Profiler PCR Array. The DEGs associated with pain and inflammation were validated by quantitative real-time polymerase chain reaction (qPCR). In addition, *Calca* ($p < 0.05$ and log2(fold change) = 0.20, Sham-vehicle vs. OVX-vehicle), which has already been reported to be increased by OVX, was also validated by qPCR.

Seventeen genes were ultimately detected through these analyses (Figure 5 and 6) and categorized into two groups: genes that showed changes in their transcriptional level by OVX (Figure 6a, b), and genes that showed changes in their transcriptional level by TPTD treatment (Figure 6c, d). Genes whose transcription was upregulated by OVX included *Calca, Tac1, Calcrl, Ptger2, P2ry14, and Penk* (Figure 6a), while those that were downregulated included *Adra2c, Grm8, Gal,* and *Ccl21* (Figure 6b). Genes whose transcription was upregulated by TPTD included *Ntf3, Bdnf, Il11, Il2rg* and *Stoml3* (Figure 6c), while those that were downregulated included *P2rx1* and *Kcnj5* (Figure 6d), although the transcription of some of these genes, such as *Bdnf, Il2rg, Stoml3* and *P2rx1*, was significantly altered by OVX.

To functionally annotate and cluster these 17 genes, we conducted the Metascape enrichment analysis as described above. The gene functional annotation obtained by this analysis is shown in a hierarchical clustering heatmap and two-dimensional functional mapping by t-SNE (Supplementary Figure 3a and b, respectively). This analysis allowed us to categorize the 17 genes into functional groups, such as CGRP-related and neuropeptides (*Calca, Calcrl, Gal* and *Tac1*), neurotrophic factors (*Ntf3* and *Bdnf*), interleukin-cytokine related (*Il11, Il2rg* and *Ccl21*), and others.

Figure 5

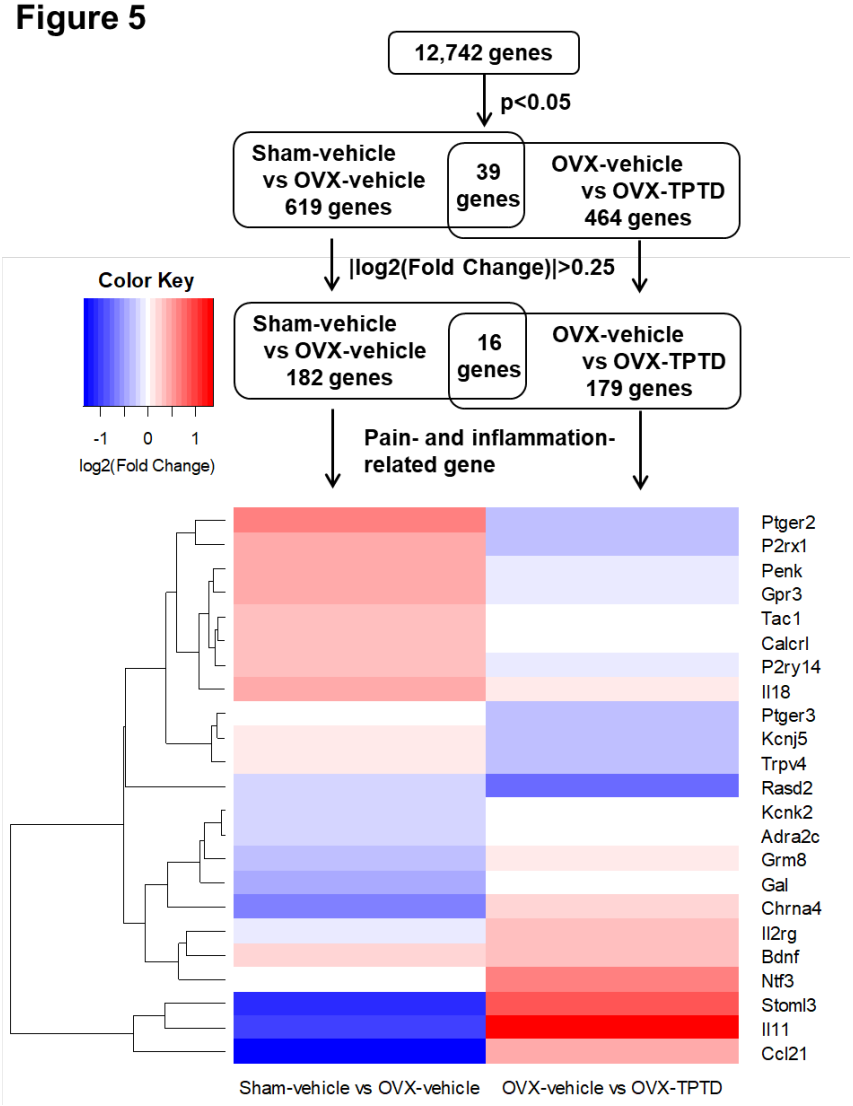

Figure 5. An analytical flowchart of gene-expression analyses by RNA-seq. RNA samples isolated from DRGs collected from the experimental groups were subjected to RNA-seq. A total of 12,742 genes were initially analyzed. Between the sham-vehicle group and OVX-vehicle group, 182 genes were identified with statistical significance and fold change, while 179 genes were identified between the OVX-vehicle group and OVX-TPTD group. Pain- and inflammation-related genes were selected from the list of the differentially expressed genes. The gene expression profiles are presented as a heatmap.

Supplementary Figure 2

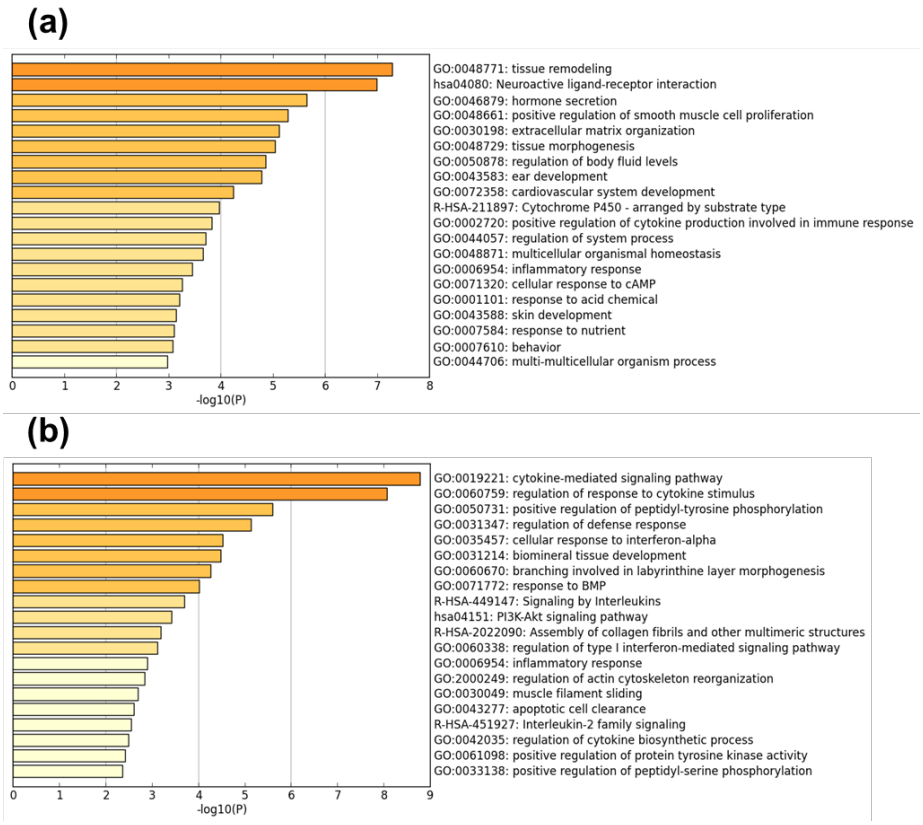

Supplementary Figure 2. A heatmap of enriched terms across input gene lists, colored by p-values. Metascape was used for the gene set enrichment analysis. (a) The DEGs between the Sham-vehicle group and the OVX-vehicle group were associated with tissue remodeling (GO:0048771) and neuroactive ligand-receptor interaction (KEGG:hsa04080). (b) The DEGs between the OVX-vehicle group and the OVX-TPTD group were associated with cytokine-mediated signaling pathways (GO:0019221) and the regulation of the response to cytokine stimuli (GO:0060759).

Figure 6

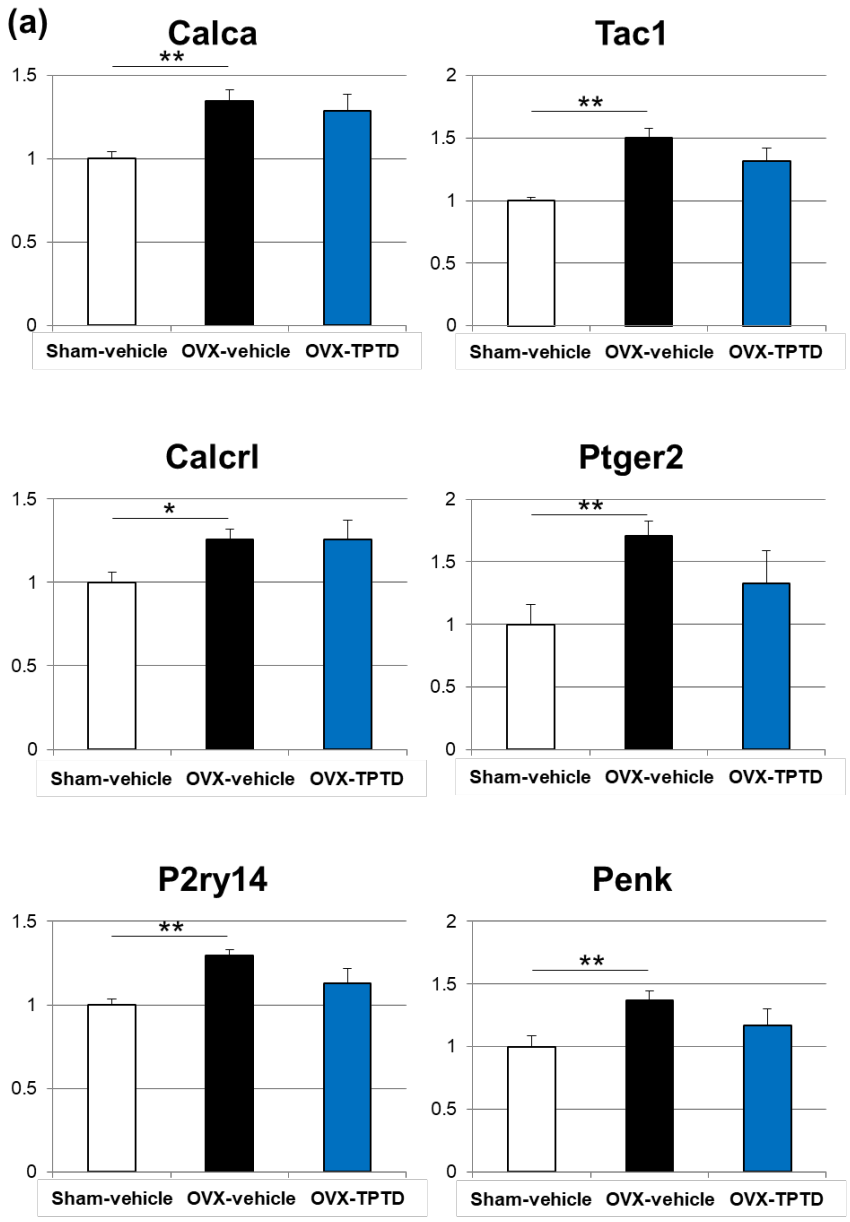
(a)
Calca
**
1.5
1
0.5
0
Sham-vehicle
OVX-vehicle
OVX-TPTD
Tac1
**
2
1.5
1
0.5
0
Sham-vehicle
OVX-vehicle
OVX-TPTD
Calcrl
*
1.5
1
0.5
0
Sham-vehicle
OVX-vehicle
OVX-TPTD
Ptger2
**
2
1.5
1
0.5
0
Sham-vehicle
OVX-vehicle
OVX-TPTD
P2ry14
**
1.5
1
0.5
0
Sham-vehicle
OVX-vehicle
OVX-TPTD
Penk
**
2
1.5
1
0.5
0
Sham-vehicle
OVX-vehicle
OVX-TPTD

(b)

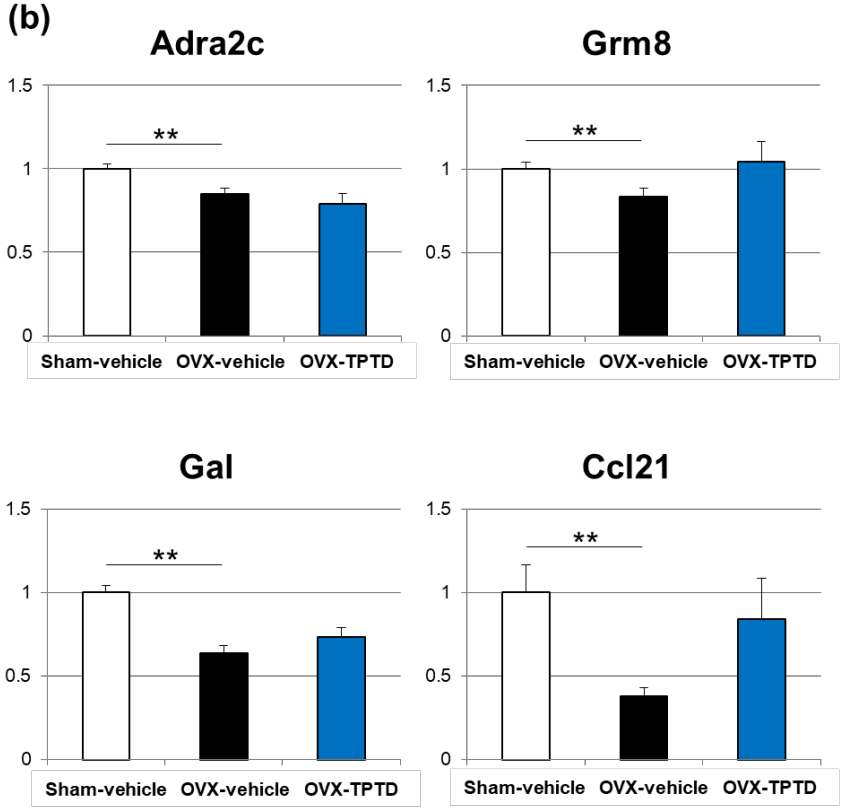
Adra2c
Grm8
Gal
Ccl21
1.5
1
0.5
0
**
Sham-vehicle
OVX-vehicle
OVX-TPTD

(c)

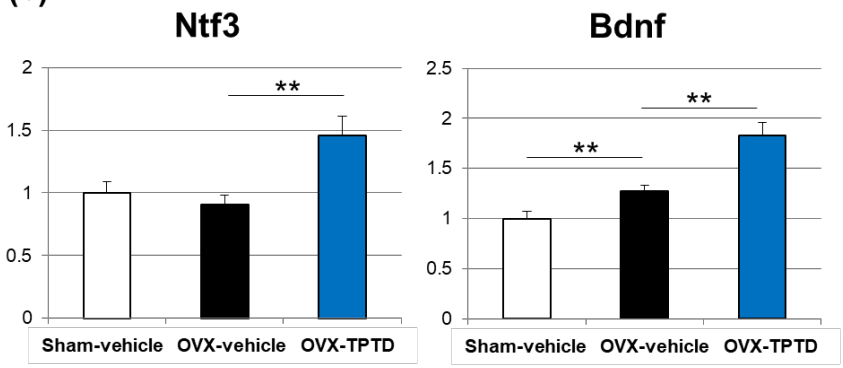
Ntf3
2
1.5
1
0.5
0
**
Sham-vehicle
OVX-vehicle
OVX-TPTD

Bdnf
2.5
2
1.5
1
0.5
0
**
**
Sham-vehicle
OVX-vehicle
OVX-TPTD

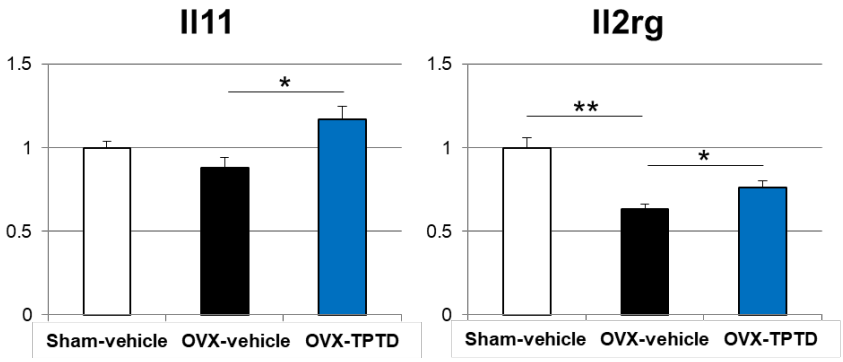
Il11
1.5
1
0.5
0
*
Sham-vehicle
OVX-vehicle
OVX-TPTD

Il2rg
1.5
1
0.5
0
**
*
Sham-vehicle
OVX-vehicle
OVX-TPTD

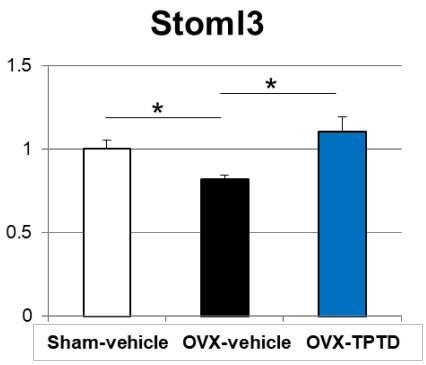
Stoml3
1.5
1
0.5
0
*
*
Sham-vehicle
OVX-vehicle
OVX-TPTD

(d)

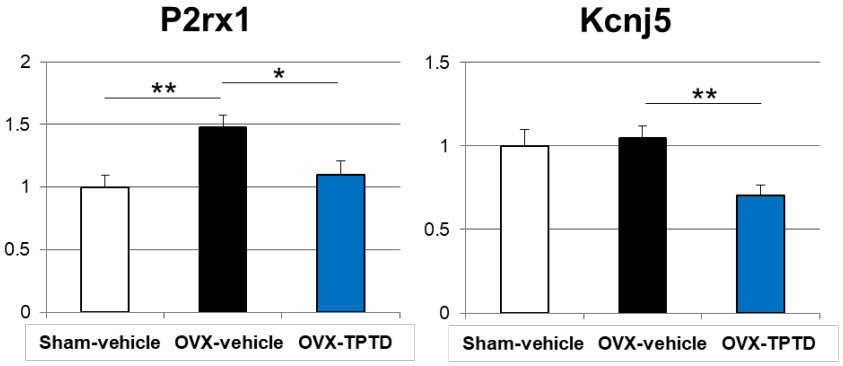
P2rx1
2
1.5
1
0.5
0
**
*
Sham-vehicle
OVX-vehicle
OVX-TPTD

Kcnj5
1.5
1
0.5
0
**
Sham-vehicle
OVX-vehicle
OVX-TPTD

Figure 6. The validation of the changes in the expression of the selected pain- and inflammation-related genes by qPCR. The differentially expressed genes associated with pain and inflammation were validated by qPCR. (a) Genes upregulated by OVX: *Calca, Tac1, Calcrl, Ptger2, P2ry14, Penk*; (b) genes downregulated by OVX: *Adra2c, Grm8, Gal, Ccl21*; (c) genes upregulated by TPTD: *Ntf3, Bdnf, Il11, Il2rg, Stoml3*; (d) genes downregulated by TPTD: *P2rx1, Kcnj5*. Significant difference: *$p < 0.05$, **$p < 0.01$. Values are normalized against the corresponding expression of *Gapdh* and relative to the Sham-vehicle group, presented as the means ± S.E.M.

Supplementary Figure 3

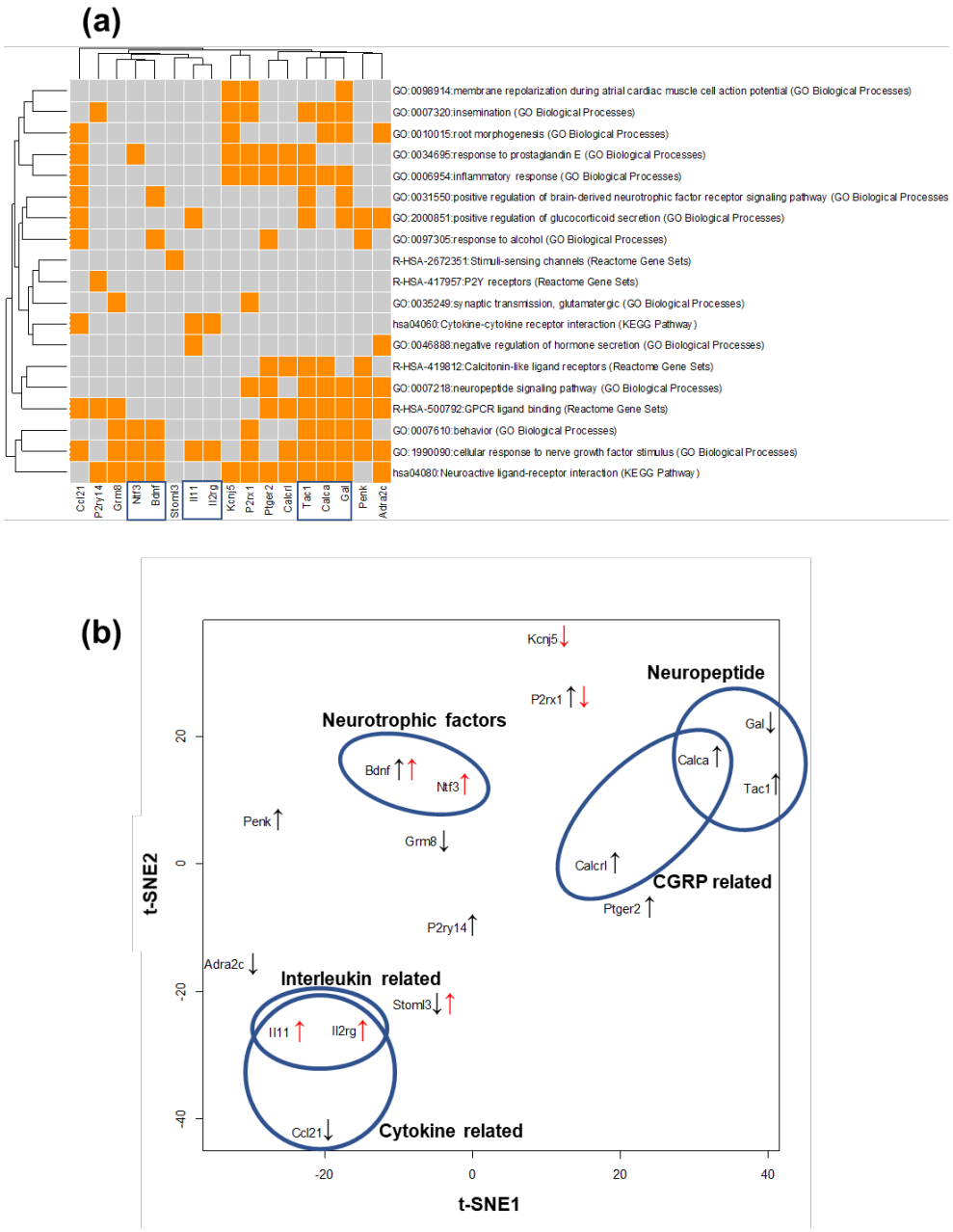

Supplementary Figure 3. Functional categorization of 17 genes that are the DEGs associated with the pain and inflammation. To functionally annotate and cluster these 17 genes, we conducted the Metascape enrichment analysis as described above. The gene functional annotation obtained by this analysis is shown in a hierarchical clustering heatmap (a) and two-dimensional functional mapping by t-SNE (b). Black arrows indicate the changes in gene expression by OVX. Red arrows indicate the changes in gene expression by TPTD

Intracellular response of DRG neurons to TPTD

To determine whether or not TPTD directly induces cellular response in the DRG neurons, we performed in vitro experiments using primary neuronal cells cultures obtained from rat DRG (Figure 7). We measured the cellular levels of cAMP and Ca^{2+}, since PTH1R is a G-protein-coupled receptor that regulates these intracellular second messengers upon activation. Treatment of the cultured rat DRG neurons with TPTD significantly decreased the cAMP levels as the TPTD concentration increased (Figure 7a), whereas the same treatment significantly increased the intracellular Ca2+ levels at TPTD doses of 10^{-4} and 10^{-5} M (Figure 7b). These data suggested that TPTD may transduce intracellular signaling in rat DRG neurons through Gαi and Gαq-coupled but not canonical Gαs signaling mediated by PTH1R in osteoblast-lineage cells.

Figure 7

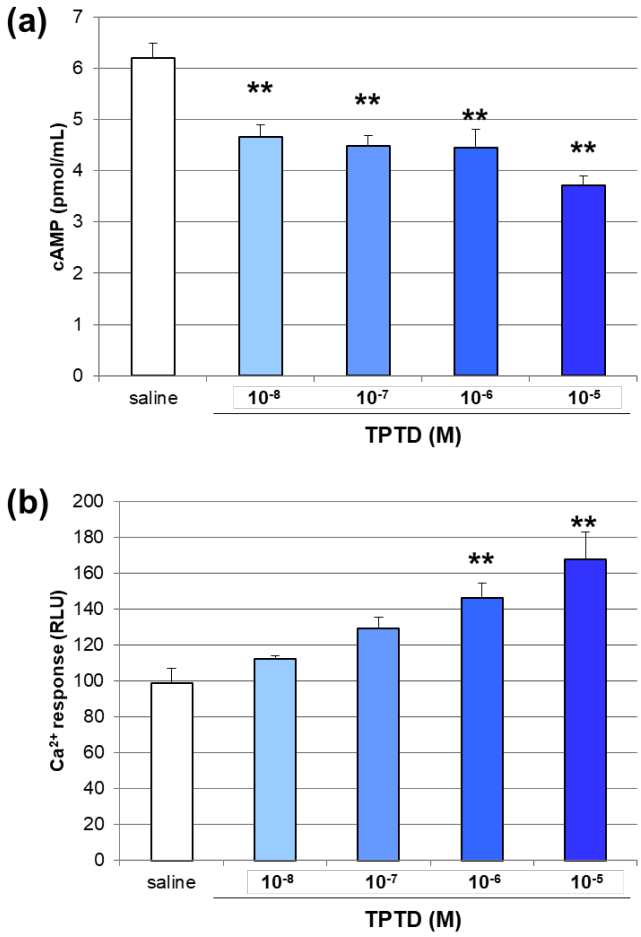

Figure 7. Cellular responses to TPTD administration in cultured DRG neurons. (a) The intracellular cAMP level in cultured DRG neurons was significantly reduced by TPTD administration as the TPTD concentration increased. (b) TPTD administration in cultured DRG neurons increased the intracellular Ca^{2+} level as the TPTD concentration increased. Significant difference: **p < 0.01.

Discussion

In this study, we applied two pain-related behavioral tests—the plantar test (paw flick test, a test observing avoidance of heat stimulation) and the von Frey test (a test to evaluate hyperalgesia by observing avoidance of mechanical stimulation)—to OVX rats to experimentally evaluate whether or not TPTD exerts an antinociceptive effect on this osteoporotic animal model, as has been observed in several clinical reports[15-25]. The plantar test showed that the withdrawal latency was gradually reduced in the OVX rats during the observation period compared with the Sham-vehicle group, confirming thermal hyperalgesia caused by OVX[8,10,11]. The reduced latency significantly recovered in the TPTD-treated OVX group starting at the initial administration compared to the OVX-vehicle group. The von Frey test also showed that the withdrawal threshold in the TPTD-treated OVX group was significantly higher than that in the vehicle-treated OVX group at four weeks after the initial administration. Therefore, we confirmed that administering TPTD to OVX rats resulted in an antinociceptive effect.

This antinociceptive effect was initiated at 6 h after administration in the plantar test. A member of our study team previously reported that the serum level of osteocalcin, an anabolic bone marker, was transiently downregulated at 6 h and then augmented 1 day after the initial TPTD administration[30]. However, in our study, the urinary CTX level was transiently increased at 6 h and then recovered to the basal level on 1 day after TPTD administration. Similar to our own study, the previous study further stated that bone histomorphometric parameters, such as osteoid surface (OS/BS) and osteoblast surface (Ob.S/BS), showed no significant changes at 8 h but did show increases by 2 days after TPTD administration. TPTD also promoted microfracture healing, but only after 2 weeks longer[31]. These findings indicate that the antinociceptive effect is exerted earlier than the bone anabolic effect by TPTD, suggesting that the pharmacological antinociceptive action of TPTD is independent of its effect on bone metabolism.

TPTD (the 1-34 fragment of human PTH) reportedly activates its cellular action effectively through rat PTH1R but poorly through rat PTH2R[32,33]. Therefore, in rats, TPTD exerts its pharmacological effects through its binding to PTH1R. Immunofluorescence against PTH1R demonstrated that most neurons in the DRG expressed substantial levels of these receptors regardless of the type of nerve fibers. The types of sensory neurons that innervate the bone are unmyelinated C-fibers and thinly myelinated Aδ-fibers, and substance P and CGRP-positive nerve fibers have been identified in bone marrow, bone cortex, and periosteum[4,34]. In a classical scheme, hyperalgesia toward both heat stimulation and mechanical stimulation is attributed to the involvement of C-fibers, while Aδ-fibers mainly transmit mechanical stimulation, although such fiber-specific function is currently controversial[35,36]. In this study, TPTD exhibited approximately the similar antinociceptive effect in both the plantar test and von Frey test.

The treatment of cultured rat DRG neurons with TPTD significantly decreased the cAMP levels and increased the Ca^{2+} levels as the TPTD concentration increased. These data suggested that PTH1R could deliver signals through a Gq and Gi-coupled downstream signaling pathway in rat DRG neurons. PTH treatment of cells expressing the Na^{+}/H^{+} exchange regulatory cofactor 2 (NHERF2)–PTH1R complex was reported to markedly activate phospholipase C and inhibit adenylyl cyclase through the stimulation of Gi protein[37]. This finding suggests that NHERF2 plays a critical role in neuronal signaling but not in osteoblastic signaling by TPTD. Consistently, NHERF2 was not detected in ROS 17/2.8 cells, a rat osteoblastic line[37]. Recent work reported that activation of PTHrP/PTH1R mediated signaling in cultured human DRGs was suggested to be involved in peripheral heat and mechanical hypersensitivity[38], suggesting opposite neural function of PTHrP and PTH although they share the same receptor; PTH1R. Their binding preferences to different conformations of PTH1R may cause distinct neuronal function as proposed in osteoblast lineage cells[39].

To understand the molecular basis of OVX-induced hyperalgesia and the antinociceptive effects of TPTD, this study investigated the functional changes in primary neurons. A transcriptome analysis by RNA-seq and successive bioinformatics showed that changes in the transcriptomal profile were associated with OVX-induced hyperalgesia and the antinociceptive effects of TPTD. On comparing the Sham-vehicle and OVX-vehicle groups, clustering of 182 significantly changed genes revealed a high association with tissue remodeling and neuroactive ligand-receptor interaction (Supplementary Figure 2a). The same comparative

analysis of 179 significantly changed genes between the OVX-vehicle and OVX-TPTD groups showed a high association with the cytokine-mediated signaling pathway and the regulation of the response to cytokine stimuli (Supplementary Figure 2b). These analyses suggest that the antinociceptive effect induced by TPTD in OVX rats involved functional changes in the cytokine pathway and cellular response to cytokines in primary sensory neurons and that TPTD did not directly restore the changes in the transcriptomal profile induced by OVX in these neurons.

We next analyzed the 17 genes that were validated by qPCR. Functional annotation and clustering divided these 17 genes into groups of CGRP-related and neuropeptides, neurotrophic factors, interleukin-cytokine related genes, and others (Supplementary Figure 3). The CGRP-related and neuropeptides included *Calca, Calcrl, Tac1,* and *Gal. Calca, Calcrl,* and *Tac1* were significantly upregulated in the OVX-vehicle group compared to the Sham-vehicle control group. It was reported that the expression of CGRP (*Calca*) and substance P (*Tac1*) in the DRG was increased by OVX. CGRP and substance P have been implicated in OVX-induced hyperalgesia[40-42]. CGRP reportedly induces hyperalgesia via the CGRP receptor, so elevated CGRP expression is suggested to produce pain[43]. Changes in the expression of CGRP and substance P by OVX were also observed in this study. Calcitonin receptor-like receptor (CLR; *Calcrl*) is a G protein-coupled receptor for CGRP. The upregulation of *Calcrl* in DRG was reportedly involved in a rat model of osteoarthritis pain[44]. Therefore, these previous findings are consistent with our results and validate our analyses of animal experiments and bioinformatics. Interestingly, in this gene group, *Gal* was the only gene that was significantly downregulated in the OVX-vehicle group. *Gal* encodes two mature peptides: galanin and galanin message-associated peptide (GMAP). *Gal*-deficient mice exhibited developmental and regenerative deficits in the DRG neurons[45]. Galanin has been reported to be involved in nociception associated with inflammatory pain[46]. These findings and our analysis suggest the mechanistic involvement of neuronal tissue damage in this skeletal pain.

The other genes that were upregulated in the OVX-vehicle group compared to the Sham-vehicle control group were *Ptger2* (encoding prostaglandin E receptor 2), *P2ry14* (purinergic receptor P2Y14) and *Penk* (Proenkephalin), all of which reportedly function in the DRG neurons and are associated with inflammatory pain and neuropathic pain[47-49]. The genes that were significantly downregulated other than *Gal* in the OVX-vehicle group included *Adra2c*, *Grm8*, and *Ccl21*. *Adra2c* encodes an alpha-2 adrenergic receptor that regulates neuronal transmission in the terminal of the DRG neurons. Therefore, the downregulation of *Adra2c* in

the DRG neurons by OVX may affect the descending pain modulatory system. *Grm8* encodes the group III metabotropic glutamate receptor that negatively modulates transient receptor potential cation channel subfamily V member 1 (TRPV1) through the inhibition of adenyl cyclase and downstream intracellular activity, thus blocking the TRPV1-induced activation of nociceptors[50]. The downregulation of *Grm8* may cause the hyper-activation of nociceptors. *Ccl21* encodes the chemokine ligand CCL12, whose upregulation is reportedly involved in neuropathic pain development[51]. Taken together, the findings from our analyses suggest that the pathogenesis of OVX-induced hyperalgesia involves the hyper-transduction of pain signals and impairment of the descending pain modulatory system as well as neuropathic tissue damage.

Given the molecular basis of the antinociceptive effect of TPTD administration to OVX rats, this pharmacological effect in the DRG neurons involved significant changes in the expression of genes that were functionally categorized into neurotrophic factors, such as *Ntf3* and *Bdnf*, and interleukin-cytokine-related factors, such as *Il11* and *Il2rg. Ntf3* and *Bdnf* encode neurotrophin-3 and brain-derived neurotrophic factor (BDNF), respectively. These factors reportedly function in DRG neurons and are associated with inflammatory and neuropathic pain[52,53]. These neurotrophic factors help support the survival of existing neurons and encourage the growth and differentiation of new neurons and synapses. Upregulation of *Bdnf* in DRG neurons of OVX group in our study was consistent with previous reports. However, TPTD treatment further augmented the level of *Bdnf*, suggesting a contradictory function of BDNF in this model. Therefore, regulatory function of BDNF should be further investigated. *Il11* encodes interleukin (IL)-11, a cytokine belonging to the IL-6 family, which has anti-inflammation properties. It was reported that treatment with IL-11 resulted in an anti-inflammatory effect in collagen-induced arthritis model mice[54]. IL-11, also referred to as a neuropoietic cytokine, influences the DRG neuron survival[55]. *Il2rg* encodes IL2RG, a component of the receptors for IL-2, IL-4, IL-7, IL-9, and IL-15. Of note, it was reported that TPTD treatment enhanced the *Il11* expression though protein kinase C (PKC) in osteoblasts[56], suggesting a direct target molecule by PTH-mediated signaling, even in the DRG neurons. Therefore, the antinociceptive effect by TPTD is suggested to be exerted partly through the induction of factors that may contribute to neuronal tissue repair in the wake of neuropathic tissue damage induced by OVX.

Stoml3 was downregulated by OVX and upregulated by TPTD administration in OVX rats in our study. *Stoml3* encodes stomatin-like protein-3 (STOML3), which modulates mechanotransduction channels and acid-sensing ion channels (ASICs). STOML3 plays important roles in several pain models; however, its function in pain seems to be paradoxical[57-59]. *P2rx1* and *Kcnj5* were significantly downregulated in the OVX-TPTD group. *P2rx1* encodes the purinergic receptor P2X1, and this gene expression was reported to be upregulated in the DRG neurons in a neuropathic pain model[60] as well as in the OVX rats in the present study. *Kcnj5* encodes G protein-activated inward rectifier potassium channel 4. *Kcnj5*-deficient mice exhibit hyperalgesia[61]. The antinociceptive effect of TPTD was partial in OVX rats. TPTD not only improved some of the genes involved in hyperalgesia, but also worsened some of them, suggesting that the antinociceptive effect of TPTD was partial. Therefore, the functional relevance of these genes in the antinociceptive effect by TPTD should be further investigated.

It has been proposed that a possible mechanism of osteoporotic pain is chronic neuronal excitation in intraosseous sensory nerve systems by acids and activated inflammatory cytokines in bone marrow environment[3,4]. Using a mouse OVX model, Dhoke et al. recently demonstrated that the antinociceptive effect by TPTD was associated with the downregulation of inflammatory cytokine expression, including IL-1β, IL-6 and TNF-α in bone tissue[62]. Osteoporotic pain involves hypoactivity of the descending inhibitory nerve system in the spinal cord that is associated with the decreased expression of serotonin receptors[3,7]. Therefore, it is will be relevant to unveil whether the pharmacological regulation in the DRG neurons of PTH is associated with the changes in the bone marrow environment and the descending inhibitory nerve system.

Our study demonstrated that TPTD administration immediately induced an antinociceptive effect in OVX rats, a timepoint that was earlier than that noted with its bone anabolic effects. This antinociceptive effect by TPTD was exerted partly through changes in the expression of genes that are associated with neuronal tissue repair. The DRG neurons expressed PTH1R, whereas TPTD mediated unique Gi and Gq signaling via PTH receptor in the cultured DRG neurons, suggesting a direct target of PTH. In conclusion, non-canonical PTH signaling in primary sensory neurons was suggested to contribute to the antinociceptive effect by TPTD in OVX rats, which involves changes in neuro-protective and inflammatory genes.

結語

今回、卵巣摘除（OVX）による骨粗鬆症モデルラットを用いて、テリパラチド（TPTD）投与による痛覚過敏に対する改善作用を検討した。

その結果、以下のことが観察された。

- OVX により生じた熱刺激に対する痛覚過敏および機械刺激に対する逃避閾値の低下は、TPTD の投与により改善した。
- 特に、経日的に評価を行った熱刺激に対する痛覚過敏は、TPTD の投与により、初回投与日（投与 6 時間後）から改善が認められ、その効果は投与終了日まで同程度を維持した。

TPTD 投与 6 時間後は、TPTD の血中濃度は低下し、骨吸収マーカーは一過的に上昇し、骨形成マーカーは一過的に低下している時間帯である [30]。したがって、TPTD による疼痛改善効果は、骨形成促進作用とは別の作用機序によってもたらされた可能性がある。

他の骨粗鬆症治療薬では、骨吸収抑制薬であるビスフォスフォネート製剤は、破骨細胞や単球、マクロファージを抑制することで、疼痛改善効果を示していると考えられている [3,8]。また、国内で骨粗鬆症の痛みに適応を持つカルシトニン製剤は、破骨細胞を抑制するとともに、セロトニン作動性下行性抑制系を賦活化することにより、疼痛改善効果を示すと考えられている [7,10,11]。

TPTD 投与後の骨吸収マーカーの動きから、TPTD による疼痛改善効果は、破骨細胞などを抑制することで疼痛改善効果を示す上記の薬剤とは異なる作用機序によって疼痛改善効果をもたらすことが考えられた。

続いて、TPTD による疼痛改善効果の神経系への分子レベルでの薬理効果を解析するため、ラットから採取した一次求心性神経の細胞体の集合である脊髄後根神経節（DRG）から RNA を抽出し、RNA-Seq 解析および種々のインフォマティクス解析を行った。これらの解析により、以下の変化が観察された。

- OVX により、疼痛関連受容体やシグナル分子に発現変動が認められた。
- TPTD の投与により、神経保護や炎症関連分子の発現変動が認められた。

さらに、蛍光免疫組織学的観察および in vitro 試験を実施し、下記を観察した。

- PTH1 型受容体は DRG の神経細胞にも発現が認められた。
- DRG から得た初代培養神経細胞への TPTD を添加した結果、細胞内 cAMP レベルが低下し、細胞内カルシウムレベルが上昇した。

以上のことから、TPTD が骨系細胞のみならず神経細胞を標的として作用し、薬理作用が示す可能性が示唆された。

現在、TPTD は臨床において、骨折リスクの高い骨粗鬆症を適応として処方されている。TPTD は、骨粗鬆症患者の腰背部痛の発生や悪化を抑制することが報告されており[15-20]、 ビスフォスフォネート製剤投与の骨粗鬆症患者の腰背部痛にも治療効果を示すことが報告されている[24]。また、TPTD の投与による腰背部痛の改善は、カルシトニン製剤よりも早期の段階で観察されることが報告されている[25]。TPTD は骨粗鬆症に伴う腰背痛に対して、投与早期には本研究で認められた痛覚過敏改善効果を示し、また、反復投与することで骨形成促進作用により椎体骨の安定化し、疼痛改善効果を示すことが考えられる。

骨粗鬆性の慢性疼痛は、顎関節や膝関節を含む変形性関節症やリウマチに伴う慢性疼痛とともに骨格性疼痛として分類される。したがって、本研究成果は、骨格性疼痛全般の病態解明や新規薬物治療の開発に貢献することが考えられる。また、今回、病態モデル動物として、卵巣摘除（OVX）ラットを用いており、エストロゲンの低下による閉経後の骨粗鬆症モデル動物としてよく用いられる。したがって、本研究成果は、閉経後の頭痛や口腔顔面痛など三叉神経支配領域における慢性疼痛の新たな病態解明に基づいた治療戦略研究への展開も期待できるものと思われる。

謝辞

本論文を結ぶにあたり、本研究を遂行する上でご指導、ご鞭撻とご援助をいただいた方々に感謝の意を表します。

北海道大学大学院歯学研究院薬理学教室教授 飯村忠浩先生には、本研究の構想からデータ解析、論文作成に至るまで、終始一貫して暖かいご指導とご鞭撻を頂きました。甚大なる感謝の意を表します。

本研究のデータ解析にあたって、たくさんの有益なご助言をいただいた愛媛大学プロテオサイエンスセンターバイオイメージング部門助教、ハーバード大学医学部ボストン小児病院研究員 李智媛先生に深く感謝いたします。

本研究の実験や解析、考察に協力いただき、細部にわたるご助言をいただいた旭化成ファーマ株式会社医薬研究センター薬理研究部主幹研究員の高尾亮子博士ならびにチームの皆様に感謝の意を表します。

本研究は旭化成ファーマ株式会社の協力を得て行われたものです。

また、ここに記しきれない多くの方々の学恩、ご支援によって本研究が成立していることを銘記し、深く感謝いたします。

References

1 Scharla, S. *et al.* Skeletal pain in postmenopausal women with osteoporosis: prevalence and course during raloxifene treatment in a prospective observational study of 6 months duration. *Current medical research and opinion* **22**, 2393-2402, doi:10.1185/030079906X154097 (2006).

2 Silverman, S. L., Piziak, V. K., Chen, P., Misurski, D. A. & Wagman, R. B. Relationship of health related quality of life to prevalent and new or worsening back pain in postmenopausal women with osteoporosis. *The Journal of rheumatology* **32**, 2405-2409 (2005).

3 Orita, S., Ohtori, S., Inoue, G. & Takahashi, K. in *Osteoporosis* (ed Yannis Dionyssiotis) Ch. 27, 541-554 (InTech, 2012).

4 Mantyh, P. W. The neurobiology of skeletal pain. *The European journal of neuroscience* **39**, 508-519, doi:10.1111/ejn.12462 (2014).

5 Yoneda, T., Hiasa, M., Nagata, Y., Okui, T. & White, F. A. Acidic microenvironment and bone pain in cancer-colonized bone. *BoneKEy reports* **4**, 690, doi:10.1038/bonekey.2015.58 (2015).

6 Ryan, P. J., Evans, P., Gibson, T. & Fogelman, I. Osteoporosis and chronic back pain: a study with single-photon emission computed tomography bone scintigraphy. *Journal of bone and mineral research : the official journal of the American Society for Bone and Mineral Research* **7**, 1455-1460, doi:10.1002/jbmr.5650071213 (1992).

7 Ito, A. *et al.* Mechanisms for ovariectomy-induced hyperalgesia and its relief by calcitonin: participation of 5-HT1A-like receptor on C-afferent terminals in substantia gelatinosa of the rat spinal cord. *The Journal of neuroscience : the official journal of the Society for Neuroscience* **20**, 6302-6308 (2000).

8 Abe, Y. *et al.* Inhibitory effect of bisphosphonate on osteoclast function contributes to improved skeletal pain in ovariectomized mice. *Journal of bone and mineral metabolism* **33**, 125-134, doi:10.1007/s00774-014-0574-x (2015).

9 Kakimoto, S. *et al.* Minodronic acid, a third-generation bisphosphonate, antagonizes purinergic P2X(2/3) receptor function and exerts an analgesic effect in pain models. *European journal of pharmacology* **589**, 98-101, doi:10.1016/j.ejphar.2008.05.011 (2008).

10 Shibata, K., Takeda, M., Ito, A., Takeda, M. & Sagai, H. Ovariectomy-induced hyperalgesia and antinociceptive effect of elcatonin, a synthetic eel calcitonin. *Pharmacology, biochemistry, and behavior* **60**, 371-376 (1998).

11 Ito, A. *et al.* Administration of estrogen shortly after ovariectomy mimics the anti-nociceptive action and change in 5-HT1A-like receptor expression induced by

calcitonin in ovariectomized rats. *Bone* **35**, 697-703, doi:10.1016/j.bone.2004.04.012 (2004).

12 Li, L. H., Wang, Z. C., Yu, J. & Zhang, Y. Q. Ovariectomy results in variable changes in nociception, mood and depression in adult female rats. *PloS one* **9**, e94312, doi:10.1371/journal.pone.0094312 (2014).

13 Forman, L. J., Tingle, V., Estilow, S. & Cater, J. The response to analgesia testing is affected by gonadal steroids in the rat. *Life sciences* **45**, 447-454 (1989).

14 Suzuki, M. *et al.* Chronic Osteoporotic Pain in Mice: Cutaneous and Deep Musculoskeletal Pain Are Partially Independent of Bone Resorption and Differentially Sensitive to Pharmacological Interventions. *Journal of osteoporosis* **2017**, 7582716, doi:10.1155/2017/7582716 (2017).

15 Genant, H. K. *et al.* The effects of teriparatide on the incidence of back pain in postmenopausal women with osteoporosis. *Current medical research and opinion* **21**, 1027-1034, doi:10.1185/030079905X49671 (2005).

16 Miller, P. D. *et al.* Longterm reduction of back pain risk in women with osteoporosis treated with teriparatide compared with alendronate. *The Journal of rheumatology* **32**, 1556-1562 (2005).

17 Langdahl, B. L. *et al.* Reduction in fracture rate and back pain and increased quality of life in postmenopausal women treated with teriparatide: 18-month data from the European Forsteo Observational Study (EFOS). *Calcified tissue international* **85**, 484-493, doi:10.1007/s00223-009-9299-6 (2009).

18 Langdahl, B. L. *et al.* Fracture Rate, Quality of Life and Back Pain in Patients with Osteoporosis Treated with Teriparatide: 24-Month Results from the Extended Forsteo Observational Study (ExFOS). *Calcified tissue international* **99**, 259-271, doi:10.1007/s00223-016-0143-5 (2016).

19 Nevitt, M. C. *et al.* Reduced risk of back pain following teriparatide treatment: a meta-analysis. *Osteoporosis international : a journal established as result of cooperation between the European Foundation for Osteoporosis and the National Osteoporosis Foundation of the USA* **17**, 273-280, doi:10.1007/s00198-005-2013-2 (2006).

20 Nevitt, M. C. *et al.* Reduction in the risk of developing back pain persists at least 30 months after discontinuation of teriparatide treatment: a meta-analysis. *Osteoporosis international : a journal established as result of cooperation between the European Foundation for Osteoporosis and the National Osteoporosis Foundation of the USA* **17**, 1630-1637, doi:10.1007/s00198-006-0177-z (2006).

21 Lyritis, G. *et al.* Back pain during different sequential treatment regimens of teriparatide: results from EUROFORS. *Current medical research and opinion* **26**, 1799-1807, doi:10.1185/03007995.2010.488516 (2010).

22 Hadji, P. *et al.* The effect of teriparatide compared with risedronate on reduction of back pain in postmenopausal women with osteoporotic vertebral fractures. *Osteoporosis international : a journal established as result of cooperation between the European Foundation for Osteoporosis and the National Osteoporosis Foundation of the USA* **23**, 2141-2150, doi:10.1007/s00198-011-1856-y (2012).

23 Tsuchie, H. *et al.* The effect of teriparatide to alleviate pain and to prevent vertebral collapse after fresh osteoporotic vertebral fracture. *Journal of bone and mineral metabolism* **34**, 86-91, doi:10.1007/s00774-014-0646-y (2016).

24 Jakob, F. *et al.* Effects of teriparatide in postmenopausal women with osteoporosis pre-treated with bisphosphonates: 36-month results from the European Forsteo Observational Study. *European journal of endocrinology / European Federation of Endocrine Societies* **166**, 87-97, doi:10.1530/EJE-11-0740 (2012).

25 Takahashi, Y. [Effect on pain with elcatonin or teriparatide for the osteoporotic vertebral fracture based on the analysis of multiple VAS data]. *The Journal of Japan Osteoporosis Society* **1**, 49-55 (2015).

26 Hargreaves, K., Dubner, R., Brown, F., Flores, C. & Joris, J. A new and sensitive method for measuring thermal nociception in cutaneous hyperalgesia. *Pain* **32**, 77-88 (1988).

27 Chaplan, S. R., Bach, F. W., Pogrel, J. W., Chung, J. M. & Yaksh, T. L. Quantitative assessment of tactile allodynia in the rat paw. *Journal of neuroscience methods* **53**, 55-63 (1994).

28 Sugie-Oya, A. *et al.* Comparison of treatment effects of teriparatide and the bisphosphonate risedronate in an aged, osteopenic, ovariectomized rat model under various clinical conditions. *Journal of bone and mineral metabolism* **34**, 303-314, doi:10.1007/s00774-015-0670-6 (2016).

29 Lacroix-Fralish, M. L., Ledoux, J. B. & Mogil, J. S. The Pain Genes Database: An interactive web browser of pain-related transgenic knockout studies. *Pain* **131**, 3 e1-4, doi:10.1016/j.pain.2007.04.041 (2007).

30 Isogai, Y. *et al.* Early Effects of Single and Low-Frequency Repeated Administration of Teriparatide, hPTH(1-34), on Bone Formation and Resorption in Ovariectomized Rats. *Calcified tissue international* **97**, 412-420, doi:10.1007/s00223-015-0026-1 (2015).

31 Sloan, A. V., Martin, J. R., Li, S. & Li, J. Parathyroid hormone and bisphosphonate have opposite effects on stress fracture repair. *Bone* **47**, 235-240, doi:10.1016/j.bone.2010.05.015 (2010).

32 Dobolyi, A., Palkovits, M. & Usdin, T. B. The TIP39-PTH2 receptor system: unique peptidergic cell groups in the brainstem and their interactions with central regulatory

mechanisms. *Progress in neurobiology* **90**, 29-59, doi:10.1016/j.pneurobio.2009.10.017 (2010).

33 Cao, Y. Q. *et al.* Primary afferent tachykinins are required to experience moderate to intense pain. *Nature* **392**, 390-394, doi:10.1038/32897 (1998).

34 Mach, D. B. *et al.* Origins of skeletal pain: sensory and sympathetic innervation of the mouse femur. *Neuroscience* **113**, 155-166 (2002).

35 Konietzny, F. Peripheral neural correlates of temperature sensations in man. *Human neurobiology* **3**, 21-32 (1984).

36 Garcia-Anoveros, J. & Corey, D. P. The molecules of mechanosensation. *Annual review of neuroscience* **20**, 567-594, doi:10.1146/annurev.neuro.20.1.567 (1997).

37 Mahon, M. J., Donowitz, M., Yun, C. C. & Segre, G. V. Na(+)/H(+) exchanger regulatory factor 2 directs parathyroid hormone 1 receptor signalling. *Nature* **417**, 858-861, doi:10.1038/nature00816 (2002).

38 Shepherd, A. J., Mickle, A. D., McIlvried, L. A., Gereau, R. W. t. & Mohapatra, D. P. Parathyroid hormone-related peptide activates and modulates TRPV1 channel in human DRG neurons. *European journal of pain* **22**, 1685-1690, doi:10.1002/ejp.1251 (2018).

39 Cheloha, R. W., Gellman, S. H., Vilardaga, J. P. & Gardella, T. J. PTH receptor-1 signalling-mechanistic insights and therapeutic prospects. *Nature reviews. Endocrinology* **11**, 712-724, doi:10.1038/nrendo.2015.139 (2015).

40 Sarajari, S. & Oblinger, M. M. Estrogen effects on pain sensitivity and neuropeptide expression in rat sensory neurons. *Experimental neurology* **224**, 163-169, doi:10.1016/j.expneurol.2010.03.006 (2010).

41 Zheng, X. F. *et al.* Blockade of substance P receptor attenuates osteoporotic pain, but not bone loss, in ovariectomized mice. *Menopause* **20**, 1074-1083, doi:10.1097/GME.0b013e31828837a6 (2013).

42 Orita, S. *et al.* The effects of risedronate and exercise on osteoporotic lumbar rat vertebrae and their sensory innervation. *Spine* **35**, 1974-1982, doi:10.1097/BRS.0b013e3181d5959e (2010).

43 Sun, R. Q. *et al.* Calcitonin gene-related peptide receptor activation produces PKA- and PKC-dependent mechanical hyperalgesia and central sensitization. *Journal of neurophysiology* **92**, 2859-2866, doi:10.1152/jn.00339.2004 (2004).

44 Bullock, C. M. *et al.* Peripheral calcitonin gene-related peptide receptor activation and mechanical sensitization of the joint in rat models of osteoarthritis pain. *Arthritis & rheumatology* **66**, 2188-2200, doi:10.1002/art.38656 (2014).

45 Holmes, F. E. *et al.* Transgenic overexpression of galanin in the dorsal root ganglia modulates pain-related behavior. *Proceedings of the National Academy of Sciences of the United States of America* **100**, 6180-6185, doi:10.1073/pnas.0937087100 (2003).

46 Ji, R. R. *et al.* Central and peripheral expression of galanin in response to inflammation. *Neuroscience* **68**, 563-576 (1995).

47 Kras, J. V., Dong, L. & Winkelstein, B. A. The prostaglandin E2 receptor, EP2, is upregulated in the dorsal root ganglion after painful cervical facet joint injury in the rat. *Spine* **38**, 217-222, doi:10.1097/BRS.0b013e3182685ba1 (2013).

48 Malin, S. A. & Molliver, D. C. Gi- and Gq-coupled ADP (P2Y) receptors act in opposition to modulate nociceptive signaling and inflammatory pain behavior. *Molecular pain* **6**, 21, doi:10.1186/1744-8069-6-21 (2010).

49 Mika, J., Rojewska, E., Makuch, W. & Przewlocka, B. Minocycline reduces the injury-induced expression of prodynorphin and pronociceptin in the dorsal root ganglion in a rat model of neuropathic pain. *Neuroscience* **165**, 1420-1428, doi:10.1016/j.neuroscience.2009.11.064 (2010).

50 Govea, R. M., Zhou, S. & Carlton, S. M. Group III metabotropic glutamate receptors and transient receptor potential vanilloid 1 co-localize and interact on nociceptors. *Neuroscience* **217**, 130-139, doi:10.1016/j.neuroscience.2012.05.014 (2012).

51 Biber, K. *et al.* Neuronal CCL21 up-regulates microglia P2X4 expression and initiates neuropathic pain development. *The EMBO journal* **30**, 1864-1873, doi:10.1038/emboj.2011.89 (2011).

52 Tu, W. *et al.* Regulation of Neurotrophin-3 and Interleukin-1beta and Inhibition of Spinal Glial Activation Contribute to the Analgesic Effect of Electroacupuncture in Chronic Neuropathic Pain States of Rats. *Evidence-based complementary and alternative medicine : eCAM* **2015**, 642081, doi:10.1155/2015/642081 (2015).

53 Gandhi, R., Ryals, J. M. & Wright, D. E. Neurotrophin-3 reverses chronic mechanical hyperalgesia induced by intramuscular acid injection. *The Journal of neuroscience : the official journal of the Society for Neuroscience* **24**, 9405-9413, doi:10.1523/JNEUROSCI.0899-04.2004 (2004).

54 Walmsley, M., Butler, D. M., Marinova-Mutafchieva, L. & Feldmann, M. An anti-inflammatory role for interleukin-11 in established murine collagen-induced arthritis. *Immunology* **95**, 31-37 (1998).

55 Thier, M., Hall, M., Heath, J. K., Pennica, D. & Weis, J. Trophic effects of cardiotrophin-1 and interleukin-11 on rat dorsal root ganglion neurons in vitro. *Brain research. Molecular brain research* **64**, 80-84 (1999).

56 Kuriwaka-Kido, R. *et al.* Parathyroid hormone (1-34) counteracts the suppression of interleukin-11 expression by glucocorticoid in murine osteoblasts: a possible

mechanism for stimulating osteoblast differentiation against glucocorticoid excess. *Endocrinology* **154**, 1156-1167, doi:10.1210/en.2013-1915 (2013).

57 Moshourab, R. A., Wetzel, C., Martinez-Salgado, C. & Lewin, G. R. Stomatin-domain protein interactions with acid-sensing ion channels modulate nociceptor mechanosensitivity. *The Journal of physiology* **591**, 5555-5574, doi:10.1113/jphysiol.2013.261180 (2013).

58 Wetzel, C. *et al.* A stomatin-domain protein essential for touch sensation in the mouse. *Nature* **445**, 206-209, doi:10.1038/nature05394 (2007).

59 Wetzel, C. *et al.* Small-molecule inhibition of STOML3 oligomerization reverses pathological mechanical hypersensitivity. *Nature neuroscience* **20**, 209-218, doi:10.1038/nn.4454 (2017).

60 Chen, L. *et al.* Differential expression of ATP-gated P2X receptors in DRG between chronic neuropathic pain and visceralgia rat models. *Purinergic signalling* **12**, 79-87, doi:10.1007/s11302-015-9481-4 (2016).

61 Marker, C. L., Cintora, S. C., Roman, M. I., Stoffel, M. & Wickman, K. Hyperalgesia and blunted morphine analgesia in G protein-gated potassium channel subunit knockout mice. *Neuroreport* **13**, 2509-2513, doi:10.1097/01.wnr.0000048541.12213.bb (2002).

62 Dohke, T. *et al.* Teriparatide rapidly improves pain-like behavior in ovariectomized mice in association with the downregulation of inflammatory cytokine expression. *Journal of bone and mineral metabolism*, doi:10.1007/s00774-017-0865-0 (2017).